Geochimica et Cosmochimica Acta 388 (2025) 182–194

Contents lists available at ScienceDirect

Geochimica et Cosmochimica Acta

journal homepage: www.elsevier.com/locate/gca

The roles of celestine and barite in modulating strontium and barium water column concentrations in the northeast Pacific Ocean

Zvi Steiner [a,*], Alexandra V. Turchyn [b], Patrizia Ziveri [c,d], Alan M. Shiller [e], Phoebe J. Lam [f], Adina Paytan [g], Eric P. Achterberg [a]

[a] GEOMAR Helmholtz Centre for Ocean Research Kiel, Wischhofstr. 1-3, 24148 Kiel, Germany
[b] Department of Earth Sciences, University of Cambridge, CB2 3EQ Cambridge, UK
[c] Institute of Environmental Science and Technology (ICTA), Autonomous University of Barcelona (UAB), Bellaterra, Barcelona, Spain
[d] Catalan Institution for Research and Advanced Studies (ICREA), 08010 Barcelona, Spain
[e] School of Ocean Science and Engineering, University of Southern Mississippi, Stennis Space Center, MS 39529, USA
[f] Department of Ocean Sciences, University of California at Santa Cruz, Santa Cruz, CA 95064, USA
[g] Earth and Planetary Sciences, University of California at Santa Cruz, Santa Cruz, CA 95064, USA

ARTICLE INFO

Associate editor: Tom Marchitto

Keywords:
Acantharia
Strontium
Barium
Barite
North Pacific
Celestite

ABSTRACT

The water column distributions of the alkaline earth metals strontium (Sr) and barium (Ba) were studied along a transect from Hawaii to Alaska. Despite similarity in the chemical properties of Sr and Ba, we find that changes in their concentrations along the transect are governed by different chemical and biological processes, meaning that these elements can be treated as independent variables in modern and ancient environments. Alaskan margin sediments are a particularly important source of dissolved Ba to the North Pacific, likely through a combination of saline submarine groundwater discharge and reductive dissolution of manganese (Mn) oxides. Abyssal North Pacific sediments are also a source of Ba to the bottom waters but a sink for Sr. We find that over 90 % of the water column variability in Sr concentrations is driven by precipitation and dissolution of the celestine ($SrSO_4$) skeletons of Acantharia. However, the high Ba content of Acantharia celestine accounts for only 5–8 % of the global ocean variability in Ba concentrations in the water column. Similarly, the effects of barite ($BaSO_4$) precipitation and/or dissolution on the marine Sr cycle is negligible, accounting for <1 % of the water column concentration structure for Sr and ~3 % of the sedimentary Sr burial. The Sr-Ba-PO_4 concentration distributions in the North Pacific are inconsistent with significant export of barite to the deep ocean and sediment. This suggests most of the barite formed at intermediate depths dissolves at similar horizons to its formation. The Ba content of phytoplankton organic matter is too low to constitute a major source for particulate Ba in the mesopelagic North Pacific, which suggests Ba is concentrated in marine aggregates by heterotrophic microorganisms.

1. Introduction

Strontium (Sr) is the fifth most abundant cation in seawater and has a residence time in the ocean of 2–3 million years (Hodell et al., 1990; Lecuyer, 2016; Richter and Turekian, 1993). Based on this long residence time one would not expect much variation in Sr concentrations in seawater, when normalized to salinity (nSr). However, measurements of seawater nSr concentrations indicate that the deep ocean is typically enriched in Sr by 2–3% relative to the surface ocean; a similar difference exists between North Atlantic Deep Water (NADW) and Antarctic Bottom Waters (AABW) (Brass and Turekian, 1974; de Villiers, 1999; Steiner et al., 2020). Concentrations of the heavier alkaline earth metal barium (Ba) also generally increase with depth, and display a non-limiting nutrient type water column distribution, and a much shorter (than Sr) residence time of 2,600–21,000 years (Horner and Crockford, 2021; Mete et al., 2023; Rahman et al., 2022).

The export of Sr from the surface to the deep ocean is understood to be mostly carried by Acantharia, a group of Rhizaria that precipitate celestine ($SrSO_4$) skeletons (Bernstein et al., 1987; De Deckker, 2004; Decelle and Not, 2015). Acantharia are highly abundant in much of the ocean, often exceeding the abundance of siliceous and calcareous Rhizaria (Radiolaria, Foraminifera) in surface waters of the subtropical

* Corresponding author.
E-mail address: zsteiner@geomar.de (Z. Steiner).

https://doi.org/10.1016/j.gca.2024.10.003
Received 15 December 2023; Accepted 3 October 2024
Available online 5 October 2024

gyres (Bishop et al., 1977; Bishop et al., 1978; Bishop and Wood, 2008; Michaels, 1988; Michaels, 1991; Michaels et al., 1995). Particularly high fluxes of Acantharia-derived celestine have been recorded in high latitude sediment traps (Belcher et al., 2018; Martin et al., 2010). After the death of the organism, the celestine shells dissolve in the water column and are not preserved in the sediment because seawater is highly undersaturated for this mineral ($\Omega_{celestine}$ = 0.1–0.2). Strontium is also incorporated in $CaCO_3$ minerals (substituting for Ca^{2+}), which are the main permanent sink for Sr in the ocean (Carpenter and Lohmann, 1992; Paytan et al., 2021; Stoll et al., 2007).

Barite ($BaSO_4$) precipitation and dissolution in the ocean may also affect the Sr distribution in the water column. Due to the physical–chemical similarities between Sr and Ba, barite incorporates up to 1 mol% of Sr in its crystal lattice (Monnin and Cividini, 2006). Barite is a highly stable mineral phase in the marine environment, that forms in association with bacterial activity within aggregates of decaying organic matter at intermediate water depths (Bishop, 1988; Ganeshram et al., 2003; Horner et al., 2017; Paytan and Griffith, 2007). The modern ocean is mostly undersaturated with respect to barite, hence it is assumed that precipitation of barite occurs within micro-environments that reach barite saturation due to release of Ba during remineralization of organic matter, dissolution of carbonate shells or other Ba carrying minerals in these microenvironments (Ganeshram et al., 2003; Gonzalez-Munoz et al., 2012; Griffith and Paytan, 2012; Rushdi et al., 2000) and binding of the Ba by extra-cellular polymeric substances excreted by bacteria (Light et al., 2023; Martinez-Ruiz et al., 2019; Torres-Crespo et al., 2015). It has also been suggested that barite and celestine accumulate within cells of diplonemid protists (Pilátová et al., 2023). A large fraction of the barite dissolves as the particles sink in the water column releasing Ba (and Sr) at depth. For example, Rahman et al. (2022) calculated that 17–46% of the excess particulate Ba, largely understood to be barite, dissolved along the South Pacific GEOTRACES GP16 transect and 58–69% dissolved along the North Atlantic GA03 transect, and Light and Norris (2021) measured a 60±20% loss of particulate barite by dissolution at intermediate water depths in the subtropical North Pacific. Lower dissolution rates are expected in the Pacific compared to the Atlantic Ocean due to a higher degree of water column barite saturation (Monnin et al., 1999). Other estimates suggest that globally ~86% of particulate Ba (largely in the form of barite) dissolves before permanent burial in the sediment (Dickens et al., 2003; Paytan et al., 1996).

Earlier studies suggested a possible connection between the abundance of Acantharia and barite formation (Bernstein et al., 1992; Bernstein et al., 1998; Bertram and Cowen, 1997). Ratios of Ba/Sr in Acantharia skeletons are higher than Ba/Sr of the ambient seawater (Bernstein et al., 1998), and Acantharia celestine seems to be the main host of mineral particulate Ba in the surface ocean (Jacquet et al., 2007a). This suggests that the remains of Acantharia could serve as a Ba-rich micro-environment that contributes to reaching barite saturation faster than the remains of other plankton (Bernstein and Byrne, 2004). However, a subsequent study in the Southern Ocean suggested that Acantharia account for ≤20 % of the total barite produced in the water column based on the standing stocks of Acantharian-associated Ba and excess particulate Ba (Jacquet et al., 2007a).

The aim of this work is to compare spatial and depth trends in dissolved Sr and Ba in the North Pacific Ocean and unravel the degree of co-variability between seawater Sr and Ba concentrations and the mechanisms that potentially couple their cycles. We hypothesize that a certain degree of co-variance between Sr and Ba in the ocean is expected due to physical–chemical similarity between the Sr^{2+} and Ba^{2+} ions, a high partition coefficient of Ba in Sr minerals and vice versa, and a potential role for celestine dissolution to contribute to barite precipitation. In addition to their link to the biological pump in the modern ocean, Sr and Ba are popular proxies of past ocean conditions, hence improved understanding of the controls over their modern distribution would facilitate and refine their interpretation as proxies of palaeoceanographic conditions.

2. Materials and methods

2.1. Sample collection

Water samples were collected during cruise CDisK-IV on board RV Kilo Moana from Hawaii to Alaska between 01-30 August 2017. Samples were collected for full water column profiles (22–39 depths per station) at six oceanographic stations from Station ALOHA (Stn. 1) in the south to Resurrection Bay (Stn. 7) in the north. Additional surface water samples were collected from the ship's underway water system. The samples were filtered through polyethersulfone (PES, Millipore) syringe filters of nominal pore size of 0.22 μm into acid cleaned low density polyethylene (LDPE; Nalgene) bottles and acidified with HNO_3 to final acid concentration of 0.02–0.04 M. Fig. 1 illustrates the locations of the sampling stations as well as temperature, salinity and density data from the cruise.

2.2. Chemical analyses

Sr/Na and Sr/Ca ratios were analyzed at the Department of Earth Sciences, University of Cambridge, using an Agilent 5100 ICP-OES by sample standard-bracketing following the method of Schrag et al. (1999) modified by Steiner et al. (2020). Calibration was done by different dilutions of IAPSO standard seawater from batch P157 that was previously analyzed for its Ca concentration using isotope dilution thermal ionization mass spectrometry (TIMS) and Sr concentration using standard additions (Steiner et al., 2020; Steiner et al., 2018). The samples and bracketing standard were diluted to salinity of 0.42 with 0.16 N HNO_3, all samples were analyzed in duplicate, and the concentrations determined based on the Sr-421.552, Ca-422.673 and Na-568.821 nm wavelengths. The average difference between duplicate analyses was 0.14% and 0.17% for Sr/Na and Sr/Ca, respectively. The long-term reproducibility of Sr/Na and Sr/Ca analyses of the IAPSO standard is 0.1% (1σ SD). Strontium concentrations were normalized to salinity of 35 PSU by multiplying the Sr/Na ratios by 0.46847 mol kg^{-1}. The salinity normalization assumes constant sodium-to-salinity ratios in the open ocean, following the modern definition of seawater salinity (Millero et al., 2008). The salinity-normalized Sr was then normalized to TEOS-10 absolute salinity of 35 g kg^{-1} (nSr), calculated using the Gibbs-Seawater Toolbox (McDougall and Barker, 2011). Normalization to salinity is done to eliminate concentration variability derived from water evaporation and precipitation because changes in salinity are the main cause of Sr concentration variability in seawater.

Barium concentrations were analyzed at GEOMAR Helmholtz Centre for Ocean Research Kiel using an Element-XR high resolution sector field inductively coupled plasma mass spectrometer (HR-ICP-MS; Thermo Fisher Scientific) in medium resolution (R = 4000). Calibration was done by standard addition; standards were prepared by adding different amounts of a Ba single element standard (Inorganic Ventures) to a North Atlantic surface water sample. Precision of the Ba analyses (2σ SD, n = 50) was 4.8 %. For intercalibration, we compared three of the CDisK-IV dissolved Ba data with those obtained at adjacent stations from the GEOTRACES GP15 section (GEOTRACES-Intermediate-Data-Product-Group, 2023; Le Roy et al., 2024), and found good agreement between the datasets (Supporting Information Fig. S1). We also compared three Station ALOHA samples from the top 400 m with three samples from the same location analyzed by Hsieh and Henderson (2017). The average concentration we analyzed was 32.1 ± 1.0 nmol kg^{-1}, slightly lower than the concentration Hsieh and Henderson reported, 33.7 ± 1.0 nmol kg^{-1}. However, the salinity of our samples was 0.3–0.6 PSU lower than the salinity Hsieh and Henderson reported, which suggests we may have sampled a different water mass at the same location.

2.3. Acantharia in North Pacific plankton tows

Vertically integrated plankton tow samples were collected at target stations during cruise CDisK-IV (Fig. 1). The plankton sampling was

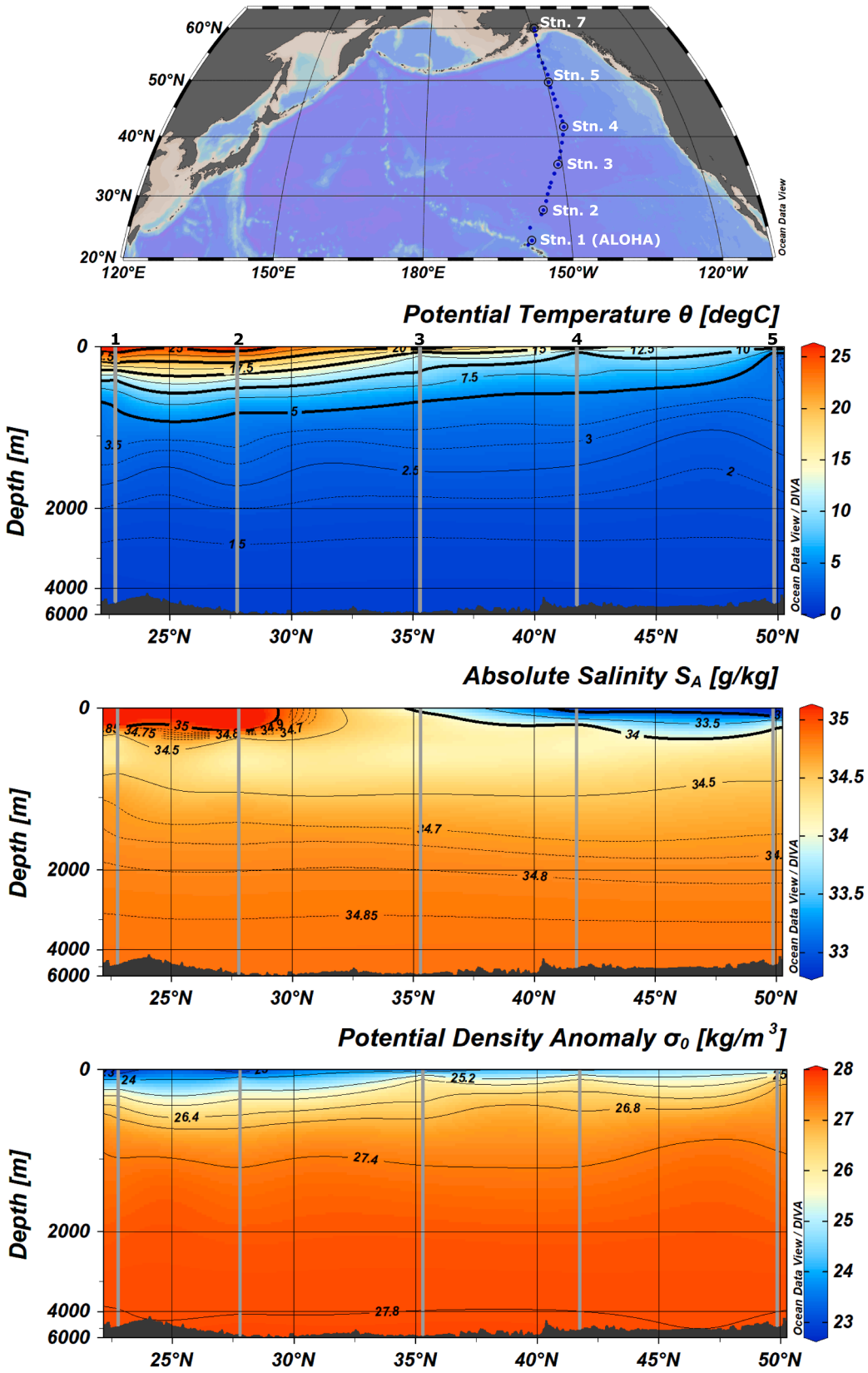

Fig. 1. Location of the sampling stations along the Hawaii to Alaska transect in the North Pacific Ocean, and TEOS-10 potential temperature, absolute salinity and potential density anomaly calculated from the cruise CTD data. Black circles in the location map mark full water column stations, blue points mark surface water samples. Note that samples were not collected at Stn. 6 due to poor weather conditions. Image plotted using Ocean Data View 5.6.3 (Schlitzer, 2020).

preceded by the deployment of a CTD cast at reference stations 1–5 to collect biogeochemical parameters. The vertically integrated plankton tows were collected at each station by using a 0.5 m net mouth diameter and a 90 μm net mesh size.

The integrated net sampling was performed from the surface down to a specified maximum depth in the water column, and then back to the surface in a continuous manner following an oblique trajectory through the water column. The target depth was determined from the fluorescence profile of the preceding CTD cast and was selected to ensure the net sampling captured well below the base of the chlorophyll maximum, and ranged from 300 m in the subtropical region to 150 m in the most northerly subpolar sites. The volume of water represented by each net tow sample was calculated by multiplying the net area by the distance travelled as determined by a flowmeter. After collection, samples were preserved in a 4% formalin seawater solution, buffered to a pH of ~8.1 with hexamethylenetetramine (Decelle et al., 2013; Massera Bottazzi et al., 1971; Michaels, 1988; Schiebel and Hemleben, 2017). Large zooplankton specimens (e.g., pteropods and heteropods (>1 mm)) were picked before splitting. Samples were split with a Folsom splitter or a McLane rotary splitter (splitting error <4%) and transferred to an ethanol solution. A portion of the sample was analyzed and Acantharia specimens were quantified using a Leica Z16 AP0 binocular light microscope at 20–100 Å~ and identified using images from Decelle and Not (2015).

3. Results

3.1. Dissolved Sr and Ba concentrations in the North Pacific

Salinity normalized Sr concentrations along the Hawaii to Alaska transect are lowest in the surface waters of the subtropical gyre and peaked at ~1000 m (Fig. 2B). Surface water nSr (~3 m below the surface), and Sr/Ca ratios, are lower in the subtropical gyre of the North Pacific and increase in the transition zone between the subtropical and subpolar gyres (Fig. 3A). The chlorophyll transition zone between the subtropical and subpolar gyres typically shifts seasonally between 32°N in winter and 42°N in summer, at the time of the CDisK-IV cruise it was at 37°N (Hou et al., 2019). The mean Sr concentration of all samples collected along this transect, normalized to TEOS-10 absolute salinity (S_A) of 35 g kg^{-1}, is 88.3 μmol kg^{-1}. The difference between the highest and lowest nSr along the transect is 2.7% (Fig. 2A), Sr/Ca ratios of seawater show similar trends to nSr and changed by 2.2% between the highest and lowest ratios along the transect (Fig. 2D). Variability in Sr/Ca is smaller than variability in nSr because Sr and Ca concentrations change with similar trends but the change in nSr relative to its background concentration is larger.

Constant shallow water Ba concentrations are observed down to 350–400 m in the subtropical gyre Stations 1–3 but only down to 100 m in subpolar gyre Station 5 (Fig. 2F), Ba concentrations then increase until ~3000 m (Fig. 2B). Despite the observed constancy in shallow water Ba concentration at each of the stations, the absolute concentration varies with latitude and increases from south to north. The northward increase, associated with the transition from the subtropical to the subpolar gyre is also observed in nSr, and to a lesser degree in Sr/Ca, but the relative increase in Ba is more pronounced as seen by the increase in surface water Ba/Sr (Fig. 3). At the northern end of the transect, close to the Alaskan shore, there is a sharp increase in surface water Ba concentrations with no similar trend in nSr (Figs. 3 and 4). In Resurrection Bay, there is a subsurface minimum in dissolved Ba concentrations at 20 m followed by a concentration maximum at 30 m (Fig. 4). There are no

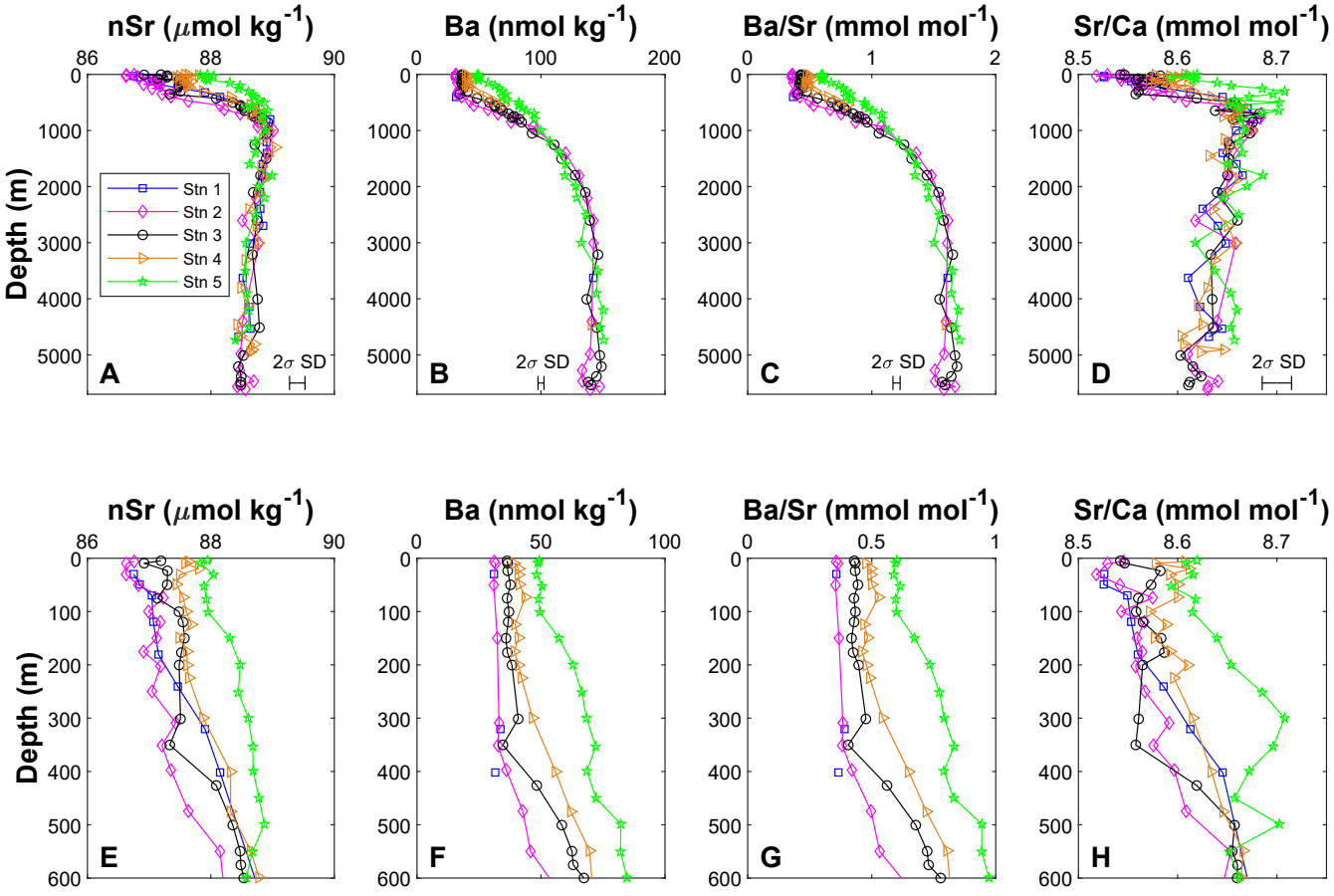

Fig. 2. Depth profiles of barium and absolute-salinity normalized strontium (nSr) concentrations for the Northeast Pacific stations. Subplots A-D present data from the full water column, subplots E-H focus on the top 600 m.

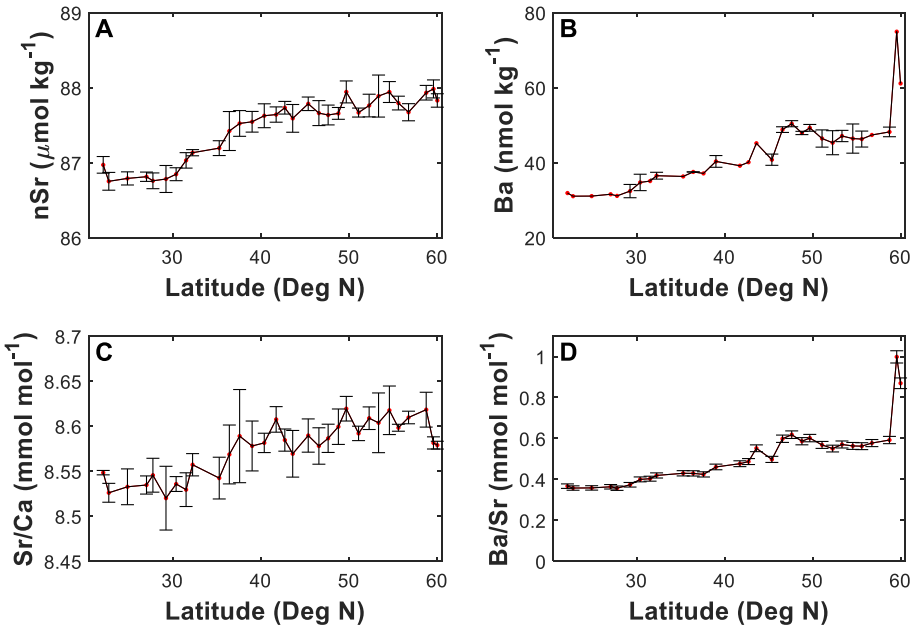

Fig. 3. Surface water concentrations along the Hawaii to Alaska transect (samples collected 2–5 m below the sea surface).

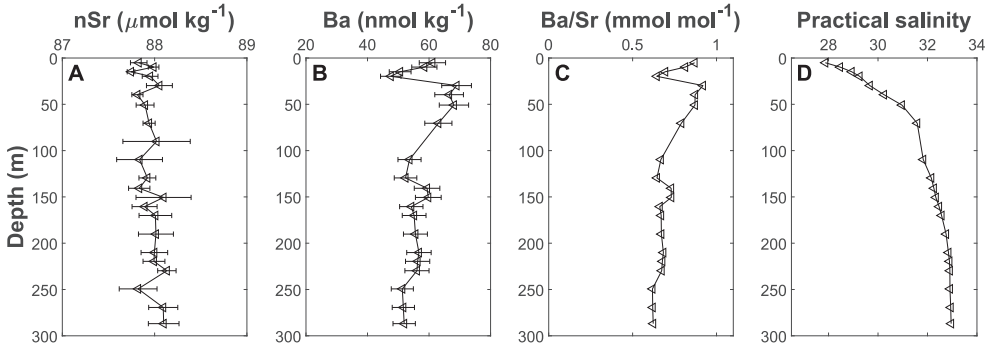

Fig. 4. Depth profiles of barium and absolute-salinity normalized strontium concentrations at Station 7, Resurrection Bay.

corresponding features in the salinity and nSr data. This Ba minimum is deeper than the chlorophyll maximum at 10 m, suggesting it could be a front of barite precipitation on decaying organic matter. Due to absence of particulate matter samples we cannot test this hypothesis.

3.2. Strontium in particulate matter

During the CDisK-IV cruise, an extensive survey of plankton net tows, shallow sediment traps, and coccolithophores from water samples collected by the CTD rosette frame equipped with Niskin bottles was undertaken in order to quantify production of $CaCO_3$ within the photic zone and export of calcified shells (Dong et al., 2019; Ziveri et al., 2023). The CDisK-IV survey revealed that during summer time, coccolithophores were the main producers of $CaCO_3$ along the transect from Hawaii to Alaska. In the subtropical gyre there was also a large flux of aragonite from pteropods to depth. Table 1 adds the Acantharia counts to the results of this survey and reveals that Acantharia were abundant in the subtropical gyre and transition zone between the subtropical and subpolar gyres. The number of Acantharia specimens collected in the subpolar gyre was very low, and they were not detected at the northern stations. The estimated abundance of Acantharia based on our survey is similar to the results of a survey in the Atlantic Ocean (Massera Bottazzi et al., 1971), however, celestine shells are highly soluble in seawater, and our Acantharia counts are lower than previous reports from the VERTEX seasonal station between California and Hawaii (33°N 139°W, Michaels, 1991). We therefore suspect that some of the shells dissolved before counting. To test this, we analyzed the concentrations of the major cations in the sample preservation solutions (Table S1). The qualitative results of the preservation solution analyses suggest that some $CaCO_3$ dissolved in the sample from Station 1, and a large amount

Table 1
Acantharia counts in plankton net tows collected in August 2017.

	Stn 1	Stn 2	Stn 2.5	Stn 3	Stn 3.5	Stn 4	Stn 4.5	Stn 5	Stn 6.5
Latitude start	22°45.247′N	27°44.451′N	31°30.644′N	35°16.346′N	38°29.710′N	41°45.714′N	45°54.011′N	49°49.285′N	58°53.701′N
Longitude	157°58.696′W	155°15.196′W	153°29.526′W	150°59.754′W	149°37.876′W	148°15.697′W	148°53.696′W	149°12.901′W	149°32.687′W
Date (dd.mm.yr)	03.08.2017	06.08.2017	11.08.2017	13.08.2017	16.08.2017	17.08.2017	20.08.2017	24.08.2017	28.08.2017
Acantharia (sp/m^3)	2300	850	770	1100	1400	840	17	0	0

of $SrSO_4$ dissolved in samples from Stations 2 and 2.5. Some $CaCO_3$ and $SrSO_4$ also dissolved in the Station 4 sample but much less than the amount dissolved in the samples from Stations 2 and 2.5. Taken together, these results support the Acantharia counts and suggest that the abundance of Acantharia is high throughout the subtropical gyre and transition zone between the gyres, and lower in the subpolar gyre.

4. Discussion

4.1. Acantharia vs. $CaCO_3$ control on strontium distribution in the North Pacific

The measured variability in nSr and Sr/Ca along the CDisK-IV transect is in agreement with the conclusion of de Villiers (1999) that the global variability in present day seawater nSr is 2–3%, but does not support claims for much larger variability in Sr/Ca in the modern ocean (Lebrato et al., 2020). Strontium is an important trace constituent in $CaCO_3$ shells, with an average partition coefficient of Sr into pteropod aragonite and planktonic foraminiferal calcite of 0.12, and ~0.3 into coccolithophore calcite, with a few exceptions such as coccolithophorid species with unusually high Sr in their shells (Carpenter and Lohmann, 1992; Elderfield et al., 1996;; Meyer et al., 2020; Milliman, 1974; Stoll and Schrag, 2000; Stoll and Ziveri, 2004). Assuming an average Sr/Ca of 0.0086 mol/mol in seawater, a Sr partition coefficient of ~0.18 in $CaCO_3$ (assuming the three main calcifying groups produce $CaCO_3$ at equal proportions) means that the average calcareous shell has a Sr/Ca of 0.0015 mol mol^{-1}. One mole of Sr is thus taken from seawater for every 667 mol of Ca when $CaCO_3$ precipitates. Assuming that the global variability in salinity normalized Ca concentration (nCa) (~1.5 mol%; Krumgalz, 1982; Steiner et al., 2021) is driven by $CaCO_3$ dissolution/precipitation, this accounts for global variability in nSr of ~0.25%, one-twelfth of the ~3% variability recorded. The remaining variability of nSr in the open ocean is mostly due to production and export of $SrSO_4$ by Acantharia (Bernstein et al., 1987; Brass and Turekian, 1974; De Deckker, 2004; de Villiers, 1999).

The celestine saturation state in the North Pacific, calculated after Rushdi et al. (2000), is as low as 0.10 at the bottom of Stations 2 and 3 and increases to 0.20 in the surface ocean at 25°C. The spatial variability in Sr^{2+} and SO_4^{2-} concentrations is small and thus seawater is always undersaturated with respect to $SrSO_4$ and differences in nSr among ocean basins are not a function of variable saturation states of celestine.

Assuming that the effect of vertical mixing is limited, the contribution of Acantharia to skeleton production relative to calcareous plankton [$SrSO_4/(SrSO_4+CaCO_3)$, in molal units] along specific isopycnals can be calculated with the following equation (Steiner et al., 2020):

$$X = 1 - \frac{1 - \frac{slope}{13.6}}{\frac{12.6 \bullet slope}{13.6} + 0.9985} \quad (1)$$

"slope" refers to the slope of a nSr-nCa property-property plot.

Eq. (1) provides a first order estimate to the mean abundance of Acantharia on a time scale of decades to centuries, depending on the age of the water mass in question. The model assumes limited mixing between water masses occupying different isopycnals. This assumption is not fully met, but mixing is weak in the deep Northeast Pacific (Hautala, 2018), and the North Pacific water column is occupied by a limited number of water masses that trace back to the same Southern Ocean end-members. Analyses of the North Pacific data along isopycnals according to Eq. (1) (Fig. 5 & Table 2) reveal that the long-term export production of Acantharia is up to 2% of the combined export of Acantharia plus calcareous organisms, which is similar to observations from

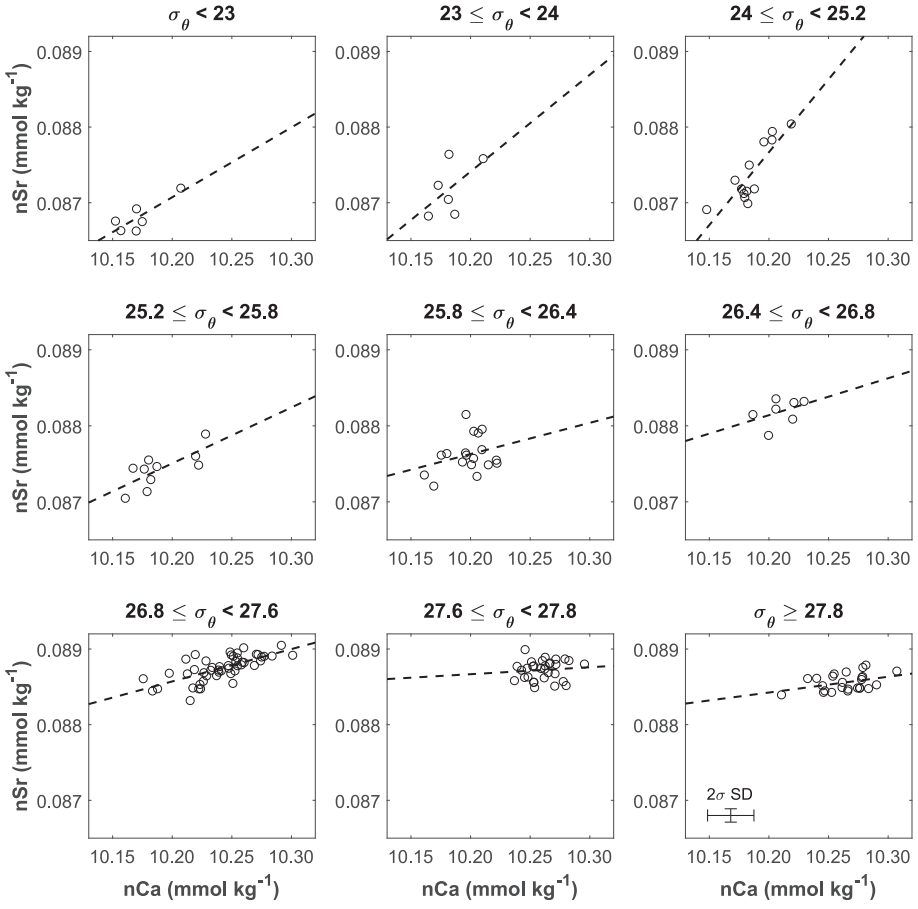

Fig. 5. nSr-nCa property-property plots along isopycnals surfaces in the North Pacific Ocean. Calcium data are from Steiner et al. (2021).

Table 2
Calculated slope of the nSr-nCa plots (from Fig. 5) and the relative molal fractions of $CaCO_3$ and $SrSO_4$ precipitating or dissolving along the main North Pacific isopycnals (Eq. (1).

	$\sigma_\theta < 23$	$23 \leq \sigma_\theta < 24$	$24 \leq \sigma_\theta < 25.2$	$25.2 \leq \sigma_\theta < 25.8$	$25.8 \leq \sigma_\theta < 26.4$	$26.4 \leq \sigma_\theta < 26.8$	$26.8 \leq \sigma_\theta < 27.6$	$27.6 \leq \sigma_\theta < 27.8$	$\sigma_\theta \geq 27.8$
Slope	0.0092	0.0128	0.0193	0.0074	0.0041	0.0049	0.0043	0.0009	0.0021
% $CaCO_3$	99.23	98.88	98.25	99.42	99.74	99.67	99.72	100	99.94
% $SrSO_4$	0.77 ± 0.31	1.12 ± 0.93	1.75 ± 0.34	0.58 ± 0.23	0.26 ± 0.33	0.33 ± 0.47	0.28 ± 0.06	0 ± 0.17	0.06 ± 0.10

the Indian and Southern oceans (Steiner et al., 2020). This small relative contribution is enough to change ocean profiles of nSr and Sr/Ca ratios by 2–3%. Higher abundance of Acantharia in the subtropical compared to the subpolar gyre (Table 1) did not appear in earlier sediment trap data from the North Pacific (Bernstein et al., 1987), suggesting either variability between years or higher $SrSO_4$ export efficiency in the subpolar gyre.

4.2. Boundary sources

Surface water concentrations of nSr in the North Pacific subpolar gyre are among the highest observed globally. Similar surface water concentrations were measured in the region of the Antarctic Circumpolar Current (ACC). The highest surface water nSr was measured near the shores of Antarctica (Steiner et al., 2020). This analogy hints at the role of upwelling in increasing the surface water nSr in the subpolar North Pacific. Recent studies have demonstrated the role of intense upwelling of intermediate waters in the north-western Pacific on the surface distribution of alkalinity and ^{14}C (Fry et al., 2016; Toggweiler et al., 2019). The nSr data do not follow the trend in salinity but closely follow the northward shoaling of low conservative temperature isothermals and potential density isopycnals (Fig. 1).

The latitudinal change in Ba concentrations supports the conclusion from the nSr and published ^{14}C data that mixing with deeper water layers contributes a significant amount of old water to the surface of the subpolar gyre. A key difference between the variability of nSr and Ba at Station 5 (4.6 degrees west of Ocean Station Papa) is that the enrichment in shallow water nSr in Station 5 compared to the other stations is limited to the top 550 m, while Ba enrichment is still observed at 1000 m (Fig. 2). If deep ventilation was responsible for Ba enrichment between 550 and 1000 m at Station 5, this would lead to the unrealistic conclusion that the effective mixing depth is different for different elements. Instead, this observation suggests an additional source for intermediate-depth Ba or a sink for Sr. We consider the option that there is a large sink for Sr at intermediate water depths less plausible since there are no known mechanisms that could effectively remove Sr at these depths.

The surface water distribution of Ba suggests there is a coastal source in the Gulf of Alaska (Fig. 3B). This is supported by data from Resurrection Bay, where we measured elevated Ba concentrations but similar nSr to the rest of the subpolar gyre (Fig. 4). This source is not observed in the GEOTRACES GP15 dataset, which does not extend as far north as the CDisK-IV cruise, likely leading to underestimation of the Alaska shelf contribution to the Ba cycle of the east North Pacific in the budget calculated by Le Roy et al. (2024). Zheng et al. (2019) identified the Aleutian Islands and Alaska Current as sources of manganese (Mn) and cobalt (Co) in the top 1000 m at 160°W. Other trace elements in the Zheng et al. dataset were not similarly enriched near Alaska (Zheng et al., 2019; Zheng et al., 2021). Given that the absence of a correlation between Ba and salinity in Resurrection Bay excludes a riverine source (Fig. 4), this suggests that release of Ba, Mn and Co from the continental shelf sediments and submarine groundwater discharge are important in the Gulf of Alaska. This is consistent with high fluxes of saline groundwater discharge by tidal pumping determined based on radon activity in the Gulf of Alaska (Dimova et al., 2015), and Ba enrichment in the North Pacific inflow to the Arctic Ocean (Whitmore et al., 2022). Similar observations of high Ba fluxes from saline submarine groundwater discharge were made in the Bay of Bengal (Moore, 1997) and western continental shelf of the North Atlantic (Rahman et al., 2022). However, this situation is different from findings from the subarctic North Atlantic, where Ba input to the upper water column was mostly associated with meteoric water (Le Roy et al., 2018). Manganese oxides have high affinity for the adsorption of Co and Ba (Murray, 1975) and are among the most energetically favorable phases for microbial oxidation of organic matter once oxygen is depleted (Froelich et al., 1979). It is therefore likely that the source for the excess Ba in the North Pacific subpolar gyre intermediate water is reductive dissolution of Mn oxides in Alaskan shelf sediments.

There is no indication in our dataset that aerosols supply any significant amount of soluble Ba or Sr to the Northeast Pacific. Aerosol fluxes along the studied transect are high between 25 and 41°N, and they have been shown to enrich the surface water with dissolved aluminum, iron and lithium (Buck et al., 2013; Steiner et al., 2022a). Barium and nSr concentrations are low in the subtropical gyre surface waters, and similar to surface water concentrations measured in other subtropical gyres (Rahman et al., 2022), with no indication of a near surface enrichment. There is also no indication in the CDisK-IV and GP15 data that the Hawaii archipelago is a significant source of dissolved Ba or Sr to the ocean (Figs. 2 and 3; GEOTRACES-Intermediate-Data-Product-Group, 2023).

Another important ocean boundary is the seafloor, and the water column profiles suggest the contribution from the sediments is markedly different for Ba and Sr in the North Pacific. In general, nSr decrease in the deep waters but Ba concentrations do not (Fig. 2). This is in accordance with porewater data from the CDisK-IV stations, which show that the sediments are a source for Ba and a sink for Sr (Steiner et al., 2023; Steiner et al., 2022b).

4.3. Strontium-barium-nutrient correlations

Strontium concentrations correlate linearly with soluble reactive phosphorous (P) at P concentrations $\geq$0.3 μmol kg^{-1} but the correlation is weak with the concentrations of silicic acid (Fig. 6A and 6B). Similar to observations from the Indian Ocean, nSr are lower in nutrient-poor North Pacific subtropical surface water samples, which we interpreted as an indication for the advantage of the mixotrophy lifestyle of Acantharia in ultra-oligotrophic conditions (Steiner et al., 2020). This argument is supported by the North Pacific plankton net data and Sr-Ca correlations, which indicate a much higher abundance of Acantharia in the P depleted subtropical gyre surface waters (Tables 1 and 2).

As in other basins, Ba concentrations correlate linearly with silicic acid at intermediate depths (Fig. 6E; Cao et al., 2016; Jacquet et al., 2007b). Deviations from the Ba-Si correlations are observed in surface waters, where Si is actively taken up by diatoms and Radiolaria while Ba is incorporated during the formation of $CaCO_3$, celestine and organic matter (Cao et al., 2020; Jacquet et al., 2007a; Mete et al., 2023). Globally, the correlation between dissolved Ba and Si is a result of the thermohaline circulation, and is set by processes in the Southern Ocean, although the chemistry of these elements is controlled by different processes (Horner et al., 2015; Le Roy et al., 2018; Lea and Boyle, 1989; Sarmiento et al., 2007) and the intracellular Ba content of diatoms is low (Sternberg et al., 2005). In North Pacific deep waters, a continuation of the linear trend that describes the intermediate water correlation predicts higher silicic acid concentrations for the observed deep-water Ba

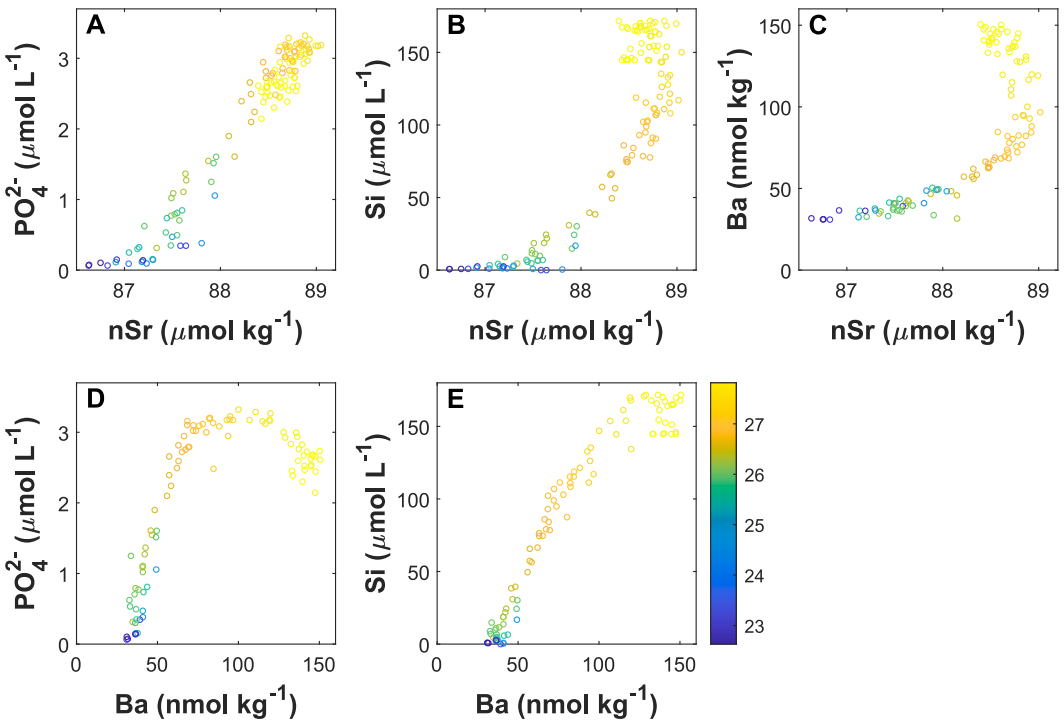

Fig. 6. Property-property plots of dissolved nSr, Ba and the macronutrients phosphate and silicic acid. Nutrient data from the CDisK-IV cruise are from (Hou et al., 2019; Steiner et al., 2021). Symbol color scaled by potential density (scale on right – kg m^{-3}).

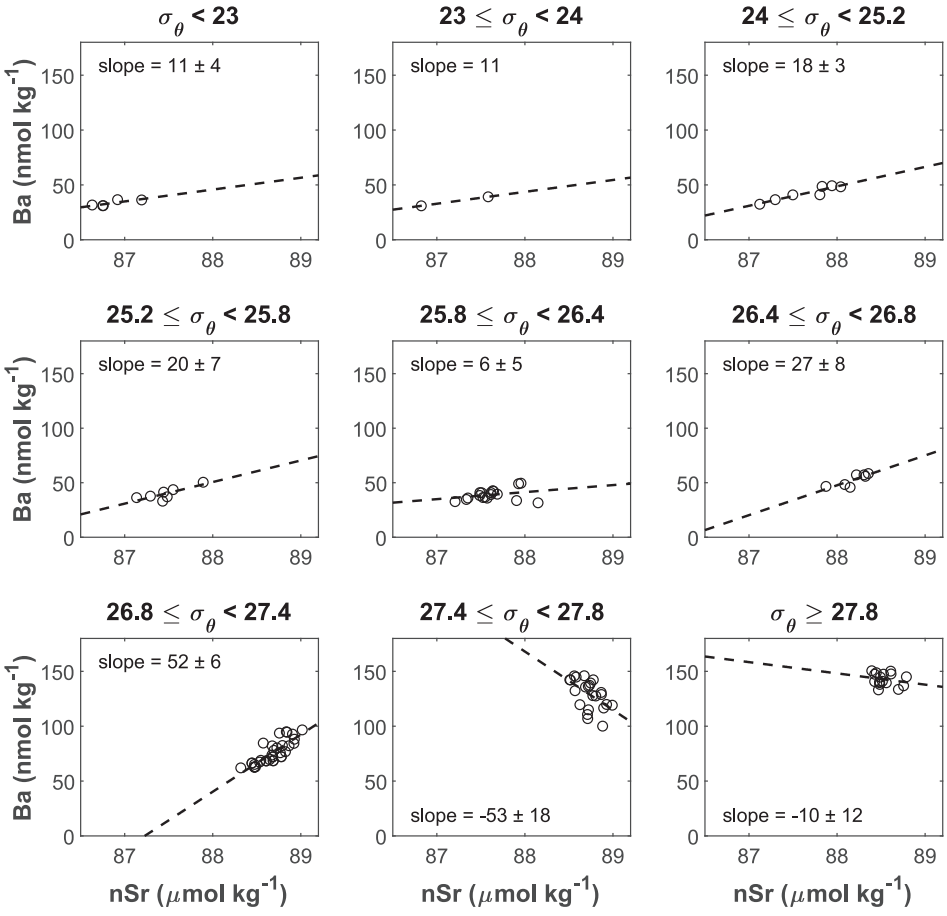

Fig. 7. Ba-nSr property-property plots along isopycnal surfaces in the North Pacific Ocean. The slope units are mmol Ba to mol Sr.

concentrations, if the distribution of these elements was controlled by the same process (Fig. 6E).

Correlations between nSr and Ba in the full dataset are non-linear (Fig. 6C). This suggests that different factors influence the Sr and Ba cycles but may not represent their real co-dependency in the North Pacific if different water masses form with diverse initial Ba/Sr. To test whether similar processes control Ba and Sr in the North Pacific we correlated their concentrations along isopycnals in Fig. 7. Strontium and Ba concentrations correlate positively in all isopycnals until 27.4, found at an average depth of 1000 m in this section, and correlate negatively between σ_θ of 27.4 and 27.8 (~1000–4000 m). The deepest water samples show no correlation between nSr and Ba.

The isopycnal correlations between Ba and nSr suggest Ba concentrations increase by 10 nmol kg^{-1} for every 1 μmol kg^{-1} increase in nSr in the subtropical gyre surface waters and by 20 nmol kg^{-1} in the water mass that outcrops in the subpolar gyre (Fig. 7). Celestine precipitated by Acantharia has on average Ba/Sr of ~3 mmol mol^{-1} (Bernstein et al., 1992), hence these correlations suggest celestine is not the main phase binding Ba in the surface North Pacific. Other phases that were shown to bind Ba are barite, Fe-Mn oxyhydroxides, aluminosilicate minerals, $CaCO_3$ and organic matter (Dehairs et al., 1980; Gonneea and Paytan, 2006). Correlations between nSr and P concentrations (Fig. 6A) suggest association with organic matter is likely the explanation for the higher slope of the Ba to nSr correlations than expected for Acantharia in the surface waters. Dependency of the Ba to nSr correlations on binding to organic matter is also consistent with the higher slopes of the correlations in the isopycnals associated with the more productive subpolar surface waters.

The slopes of the correlation between Ba and nSr increase in the intermediate waters in the σ_θ range of 26.4–27.4, corresponding to the depth range of 100–150 m at Stn. 5 and 400 m to 1000 m at Stn. 1 (Fig. 7). This is the depth range where most of the attenuation in organic matter flux occurs and where barite is expected to form in the water column (Bishop, 1988; Dehairs et al., 2008; van Beek et al., 2007). Averyt and Paytan (2003) measured Sr/Ba of 33±5 mmol mol^{-1} (or Ba/Sr of 30 mol mol^{-1}) in barite samples collected in core tops from various locations. A higher Sr content may be associated with poorly crystalline barite but this barite dissolves faster and is not preserved in core tops. The core top Sr content of barite translates to a steep increase in Ba relative to Sr that will visually appear nearly vertical in the correlations presented in Fig. 8. In fact, the partition coefficient of Sr in marine barite suggests that if the complete range of Ba water column variability in the North Pacific, 120 nmol kg^{-1}, is stored and released from barite mineral precipitation and dissolution, that would translate to a change in nSr of only 4 nmol kg^{-1}, which is undetectable by our analytical method. The slopes of the Ba to nSr correlations in our data thus is too low to be controlled by precipitation and dissolution of barite.

Diapycnal Ba variability correlates very well with P until σ_θ of 27.4, roughly located at 1000 m along the transect (Fig. 8), this suggests Ba export is associated with export of organic matter as suggested by Dymond et al., (1992). $CaCO_3$ minerals also carry Ba and Sr but do not explain the observed Sr-to-Ba trends because the Sr and Ba partition coefficient into foraminiferal shells are similar (Elderfield et al., 1996; Lea and Boyle, 1989), and the partition coefficient of Sr into coccoliths is

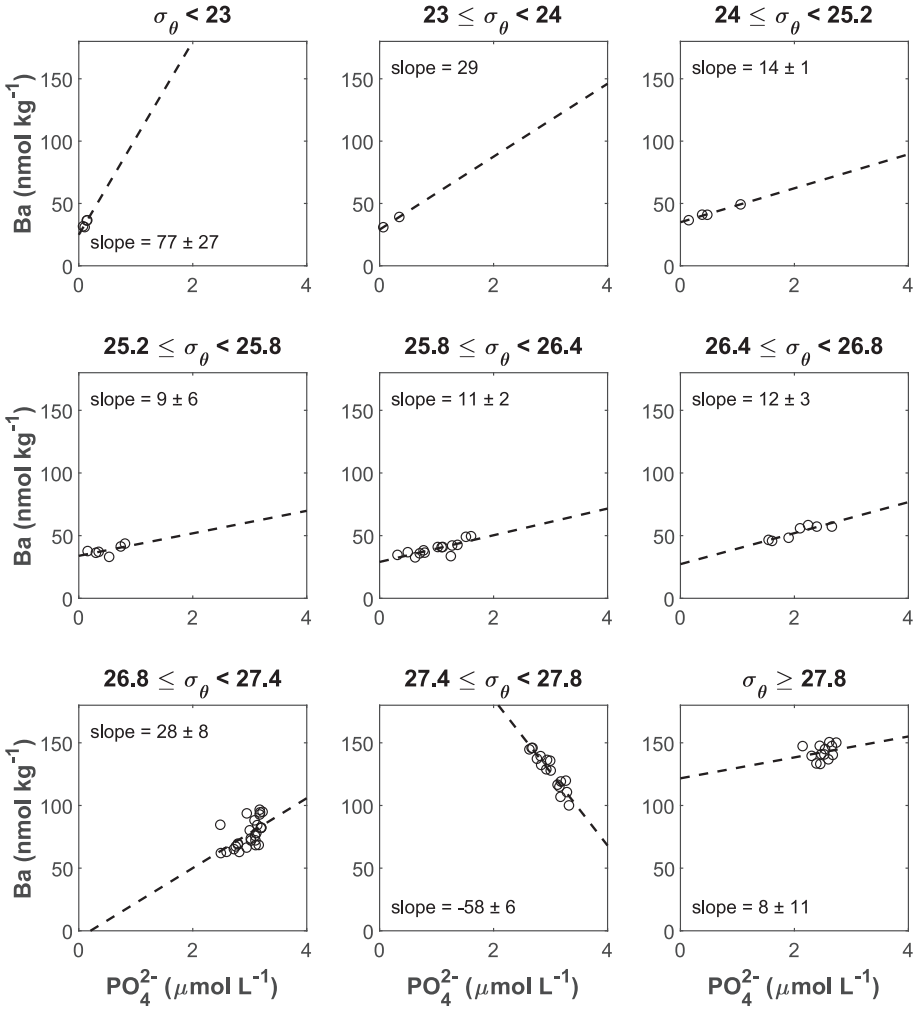

Fig. 8. Barium-phosphate property-property plots along isopycnals surfaces in the North Pacific Ocean. The slope units are mmol Ba to mol P.

~3 times larger than the partition coefficient of Ba (Langer et al., 2009), hence shells formed in the surface ocean should contain relatively little Ba and produce lower slopes than observed in the Sr-Ba correlations.

4.4. Particulate barium

Suspended particles were collected along a similar Hawaii-to-Alaska transect during the GEOTRACES GP15 expedition. The GP15 samples were digested for their total Ba and P content (Lam et al., 2024). Total particulate Ba includes Ba associated with organic matter, $CaCO_3$, celestine, metal oxides, lithogenic material, and barite.

The particulate data suggest Ba is mostly associated with the smaller particles that settle slowly in the water column; Ba concentrations are very low in particles larger than 51 μm (Fig. 9A). This is consistent with particulate Ba being dominated by very small marine barite particles (Dehairs et al., 1980), and with a low export efficiency as calculated in the previous sections using the dissolved Ba concentrations. The other observation is that while particulate Ba concentrations in the photic zone are extremely low, particulate Ba concentrations increase in the mesopelagic zone (Fig. 9 A and B). This observation is in-line with the proposed transfer of Ba from the dissolved to the particulate fractions at depths where much of the sinking organic matter is remineralized, but contradicts the hypothesis that algal organic matter is the main source of Ba for the formation of barite given the low particulate Ba/P ratios in the photic zone (<1 mmol mol^{-1}; Fig. 9D), and in diatom cells (0.5 μmol mol^{-1} according to Sternberg et al., 2005). Horner et al. (2015) reached a similar conclusion that organic matter is not a substantial carrier of Ba in the water column using data from the South Atlantic.

If organic matter does not supply enough Ba for production of barite, the Ba has to be extracted from the surrounding seawater at the sites of barite precipitation. It was previously shown that barite forms on specific organic templates derived from microbial extractions (Martinez-Ruiz et al., 2019; Torres-Crespo et al., 2015). The saturation horizon for marine barite is at >1000 m near Hawaii and shoals to <500 m in the subpolar gyre (Le Roy et al., 2024), hence the accumulation of Ba in particulate material mostly happens in undersaturated waters and most of it is released and dissolves before or upon reaching saturated waters (Fig. 9 A-B). This observation necessitates biological control over the release of Ba, in addition to its uptake.

5. Implications

High barite to labile Ba ratio in suspended particles suggest barite is generated in the upper North Pacific water column (van Beek et al., 2022). On the other hand, limited importance of barite in Ba export, calculated here using the Sr-Ba correlations, is consistent with visual observations of barite dissolution in the top 1000 m (Light and Norris, 2021), high regeneration rates of Ba in the intermediate to deep parts of the water column, calculated using North Pacific Ba isotope data (Hsieh and Henderson, 2017; Yu et al., 2022) and low barite accumulation rates in sediments of this region (Eagle et al., 2003). Dissolved concentration ratios are sensitive to export but not to recycling, as long as the particulate concentrations are low relative to the dissolved concentrations, which is the normal case for Ba in the ocean (Dehairs et al., 2008; van Beek et al., 2007), and therefore do not inform on formation and dissolution of mineral phases if they happen along the same horizon. This comparison between the different methods used to quantify the oceanic Ba cycle suggests barite continuously forms in the North Pacific intermediate waters but its export efficiency is low. The conclusion that most barite forms at the depth it is found in the intermediate water column with limited vertical transport is consistent with measurements of radium isotopes in suspended particulate matter from the Sargasso Sea (van Beek et al., 2007).

It is likely that initially, particulate phases such as organic matter and Mn-oxides are important for particulate Ba enrichment but this Ba along with Ba from seawater is incorporated into poorly crystallized or micro-crystalline barite. The micro-crystalline barite is possibly more soluble than predicted from published solubility relations because of the presence of impurities such as Sr (Rushdi et al., 2000), and because those solubility relations are based on experiments with lab-made, coarse-grained barite, which may not wholly represent micro-crystalline barite (Mete et al., 2023). Support for existence of barite minerals with various solubilities comes from observations that barite recrystallizes after burial in North and Equatorial Pacific sediments (Middleton et al., 2023; Steiner et al., 2023). Barite may still be enriched relative to other minerals in North Pacific sediments underlying productive surface waters because low preservation of phases like $CaCO_3$ and organic matter in these sediments results in very low sedimentation and burial rates of these phases (Kemnitz et al., 2022).

The global flux of Ba from the surface to deep ocean is ~100 Gmol y^{-1}, of this ~85 Gmol y^{-1} dissolves in the water column while 15–19 Gmol y^{-1} is buried (Carter et al., 2020; Dickens et al., 2003; Paytan and Kastner, 1996; Rahman et al., 2022). Assuming a Sr/Ba of 33±5 mmol mol^{-1} in marine barites (Averyt and Paytan, 2003) this suggests a burial flux of Sr associated with marine barite of 0.6±0.2 Gmol y^{-1}. Some marine barite minerals have higher Sr/Ba, up to 50–60 mmol mol^{-1}, which may represent phases that are more common in the water column (van Beek et al., 2003; Wu et al., 2022), hence Sr export associated with marine barite is ≤6 Gmol y^{-1}. For comparison, the global removal flux of Sr from the ocean by burial of $CaCO_3$ is estimated at 174 Gmol y^{-1}, of which 20 Gmol y^{-1} is buried in deep-sea sediments (Paytan et al., 2021), and >90% of the water column remineralization of Sr is associated with Acantharia celestine. Therefore, barite accounts for <1% of the Sr export flux and ~3% of the burial of Sr in deep-sea sediments. Although each of these fluxes and ratios is subject to considerable uncertainty, the conclusion of minimal impact of barite on Sr transport seems robust.

The flux associated with Acantharia does not lead to permanent burial of Sr and Ba but adds a vector for Ba transport in the water

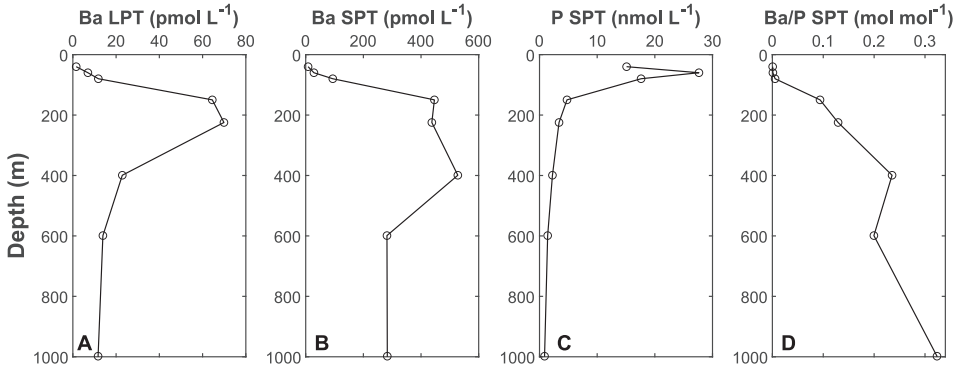

Fig. 9. Particulate Ba and P concentrations measured at Stn. 10 of the US GEOTRACES GP15 transect, 42°N 152°W (Lam et al., 2024). LPT is total particulate in the >51 μm size fraction, SPT is total particulate in the 0.8–51 μm size fraction.

column. Acantharia are responsible for most of the ~3 μmol kg^{-1} variability in nSr concentrations in the ocean. Assuming a Ba/Sr ratio of 3 mmol mol^{-1} in Acantharia celestine (Bernstein et al., 1992), this suggests that Acantharia directly account for 6–9 nmol kg^{-1} variability in Ba concentration, which is 5–8% of the global water column variability. Rahman et al. (2022) concluded that most of the vertical Ba gradient is due to conservative mixing of waters with differing 'preformed Ba', which suggests Acantharia could be very important for upper water column non-conservative changes in Ba. The importance of Acantharia in water column variability of Ba is larger in the top 1000 m but is typically negligible below 1000 m. The indirect effect of Acantharia on Ba burial may be larger if the remains of Acantharia are disproportionally important for barite formation (Bernstein and Byrne, 2004; Bernstein et al., 1998). However, the North Pacific plankton net and water chemistry data suggest Acantharia are more abundant in the oligotrophic subtropical gyre. The sediment Ba content, on the other hand, is highest in Station 4, followed by Station 5, and lower in the Stations underlying the subtropical gyre (Steiner et al., 2023). If the remains of Acantharia were important for Ba burial, sedimentary Ba concentrations would have been higher in sediments underlying less productive ocean regions. Observations that sedimentary barite correlate with ocean productivity (Dymond et al., 1992; Francois et al., 1995) suggest barite formation is independent of the abundance of Acantharia. In summary, the findings of this work suggest Ba and Sr can be treated as independent variables that are commonly not affected by the same biological and chemical processes.

Data availability

Data are available through PANGAEA at https://doi.org/10.1594/PANGAEA.964813.

CRediT authorship contribution statement

Zvi Steiner: Writing – review & editing, Writing – original draft, Validation, Resources, Project administration, Methodology, Investigation, Funding acquisition, Formal analysis, Data curation, Conceptualization. **Alexandra V. Turchyn:** Writing – review & editing, Resources. **Patrizia Ziveri:** Writing – review & editing, Investigation. **Alan M. Shiller:** Writing – review & editing. **Phoebe J. Lam:** Investigation. **Adina Paytan:** Writing – review & editing. **Eric P. Achterberg:** Writing – review & editing, Resources.

Declaration of competing interest

The authors declare that they have no known competing financial interests or personal relationships that could have appeared to influence the work reported in this paper.

Acknowledgements

This work was funded by Deutsche Forschungsgemeinschaft (DFG) grant number 458035111 to ZS. We thank Jess Adkins and William Berelson, chief scientists of cruise CDisK-IV, for inviting ZS and PZ to participate in the cruise, and Griselda Anglada for her help with sample processing at ICTA-UAB. Collection and analysis of the GP15 data was made possible by US NSF award 1736601 to PJL. We thank Tristan Horner, Jiawang Wu and an anonymous reviewer for their comments that helped improve the manuscript.

Appendix A. Supplementary material

The supplementary material compares the CDisK-IV data and available data from the North Pacific Ocean. Figure S1 compares the CDisK-IV Ba data and Ba data from the GEOTRACES GP15 section (GEOTRACES-Intermediate-Data-Product-Group, 2023). Figure S2 compares the CDisK-IV Sr data and Sr data published in Bernstein et al. (1987) and de Villiers (1999). Table S1 presents Sr and Ca concentrations in the solutions used for preservation of specimens picked from the plankton net tows. Supplementary material to this article can be found online at https://doi.org/10.1016/j.gca.2024.10.003.

References

Averyt, K.B., Paytan, A., 2003. Empirical partition coefficients for Sr and Ca in marine barite: Implications for reconstructing seawater Sr and Ca concentrations. Geochem. Geophys. Geosyst. 4 (5).
Belcher, A., Manno, C., Thorpe, S., Tarling, G., 2018. Acantharian cysts: high flux occurrence in the bathypelagic zone of the Scotia Sea. Southern Ocean. Mar. Biol. 165 (7), 117.
Bernstein, R.E., Betzer, P.R., Feely, R.A., Byrne, R.H., Lamb, M.F., Michaels, A.F., 1987. Acantharian fluxes and strontium to chlorinity ratios in the North Pacific Ocean. Science 237 (4821), 1490–1494.
Bernstein, R.E., Byrne, R.H., 2004. Acantharians and marine barite. Mar. Chem. 86 (1), 45–50.
Bernstein, R.E., Byrne, R.H., Betzer, P.R., Greco, A.M., 1992. Morphologies and transformations of celestite in seawater: The role of acantharians in strontium and barium geochemistry. Geochim. Cosmochim. Acta 56 (8), 3273–3279.
Bernstein, R.E., Byrne, R.H., Schijf, J., 1998. Acantharians: a missing link in the oceanic biogeochemistry of barium. Deep-Sea Res. I 45 (2), 491–505.
Bertram, M.A., Cowen, J.P., 1997. Morphological and compositional evidence for biotic precipitation of marine barite. J. Mar. Res. 55 (3), 577–593.
Bishop, J.K.B., 1988. The barite-opal-organic carbon association in oceanic particulate matter. Nature 332 (6162), 341–343.
Bishop, J.K.B., Edmond, J.M., Ketten, D.R., Bacon, M.P., Silker, W.B., 1977. The chemistry, biology, and vertical flux of particulate matter from the upper 400 m of the equatorial Atlantic Ocean. Deep-Sea Res. 24 (6), 511–548.
Bishop, J.K.B., Ketten, D.R., Edmond, J.M., 1978. The chemistry, biology and vertical flux of particulate matter from the upper 400 m of the Cape Basin in the southeast Atlantic Ocean. Deep-Sea Res. 25 (12), 1121–1161.
Bishop, J.K.B., Wood, T.J., 2008. Particulate matter chemistry and dynamics in the twilight zone at VERTIGO ALOHA and K2 sites. Deep-Sea Res. I 55 (12), 1684–1706.
Brass, G.W., Turekian, K.K., 1974. Strontium distribution in GEOSECS oceanic profiles. Earth Planet. Sci. Lett. 23 (1), 141–148.
Buck, C.S., Landing, W.M., Resing, J., 2013. Pacific Ocean aerosols: Deposition and solubility of iron, aluminum, and other trace elements. Mar. Chem. 157, 117–130.
Cao, Z., Siebert, C., Hathorne, E.C., Dai, M., Frank, M., 2016. Constraining the oceanic barium cycle with stable barium isotopes. Earth Planet. Sci. Lett. 434, 1–9.
Cao, Z., Li, Y., Rao, X., Yu, Y., Hathorne, E.C., Siebert, C., Dai, M., Frank, M., 2020. Constraining barium isotope fractionation in the upper water column of the South China Sea. Geochim. Cosmochim. Acta 288, 120–137.
Carpenter, S.J., Lohmann, K.C., 1992. Sr/Mg ratios of modern marine calcite: Empirical indicators of ocean chemistry and precipitation rate. Geochim. Cosmochim. Acta 56 (5), 1837–1849.
Carter, S.C., Paytan, A., Griffith, E.M., 2020. Toward an improved understanding of the marine barium cycle and the application of marine barite as a paleoproductivity proxy. Minerals 10 (5).
De Deckker, P., 2004. On the celestite-secreting Acantharia and their effect on seawater strontium to calcium ratios. Hydrobiologia 517 (1–3), 1–13.
de Villiers, S., 1999. Seawater strontium and Sr/Ca variability in the Atlantic and Pacific oceans. Earth Planet. Sci. Lett. 171 (4), 623–634.
Decelle, J., Martin, P., Paborstava, K., Pond, D.W., Tarling, G., Mahe, F., de Vargas, C., Lampitt, R., Not, F., 2013. Diversity, Ecology and Biogeochemistry of Cyst-Forming Acantharia (Radiolaria) in the Oceans. PLoS One 8 (1).
Decelle, J., Not, F., 2015. Acantharia, eLS. John Wiley & Sons Ltd, Chichester, pp. 1–10.
Dehairs, F., Chesselet, R., Jedwab, J., 1980. Discrete suspended particles of barite and the barium cycle in the open ocean. Earth Planet. Sci. Lett. 49 (2), 528–550.
Dehairs, F., Jacquet, S.H.M., Savoye, N., Van Mooy, B.A.S., Buesseler, K.O., Bishop, J.K.B., Lamborg, C.H., Elskens, M., Baeyens, W., Boyd, P.W., Casciotti, K.L., Monnin, C., 2008. Barium in twilight zone suspended matter as a potential proxy for particulate organic carbon remineralization: results for the North Pacific. Deep Sea Res. II 55 (14), 1673–1683.
Dickens, G.R., Fewless, T., Thomas, E., Bralower, T.J., 2003. Excess barite accumulation during the Paleocene-Eocene thermal Maximum: Massive input of dissolved barium from seafloor gas hydrate reservoirs. In: Wing, S.L., Gingerich, P.D., Schmitz, B., Thomas, E. (Eds.), Causes and consequences of globally warm climates in the early Paleogene. Geol. Soc. Am. Bull., pp. 11–23.
Dimova, N.T., Paytan, A., Kessler, J.D., Sparrow, K.J., Garcia-Tigreros Kodovska, F., Lecher, A.L., Murray, J., Tulaczyk, S.M., 2015. Current magnitude and mechanisms of groundwater discharge in the Arctic: Case study from Alaska. Env. Sci. Tech. 49 (20), 12036–12043.
Dong, S., Berelson, W.M., Rollins, N.E., Subhas, A.V., Naviaux, J.D., Celestian, A.J., Liu, X., Turaga, N., Kemnitz, N.J., Byrne, R.H., Adkins, J.F., 2019. Aragonite dissolution kinetics and calcite/aragonite ratios in sinking and suspended particles in the North Pacific. Earth Planet. Sci. Lett. 515, 1–12.
Dymond, J., Suess, E., Lyle, M., 1992. Barium in deep-sea sediment: a geochemical proxy for paleoproductivity. Paleoceanography 7 (2), 163–181.
Eagle, M., Paytan, A., Arrigo, K.R., van Dijken, G., Murray, R.W., 2003. A comparison between excess barium and barite as indicators of carbon export. Paleoceanography 18 (1), 1021.

Elderfield, H., Bertram, C.J., Erez, J., 1996. Biomineralization model for the incorporation of trace elements into foraminiferal calcium carbonate. Earth Planet. Sci. Lett. 142 (3–4), 409–423.
Francois, R., Honjo, S., Manganini, S.J., Ravizza, G.E., 1995. Biogenic barium fluxes to the deep sea: Implications for paleoproductivity reconstruction. Glob. Biogeochem. Cycle 9 (2), 289–303.
Froelich, P.N., Klinkhammer, G.P., Bender, M.L., Luedtke, N.A., Heath, G.R., Cullen, D., Dauphin, P., Hammond, D., Hartman, B., Maynard, V., 1979. Early oxidation of organic matter in pelagic sediments of the eastern equatorial Atlantic: Suboxic diagenesis. Geochim. Cosmochim. Acta 43 (7), 1075–1090.
Fry, C.H., Tyrrell, T., Achterberg, E.P., 2016. Analysis of longitudinal variations in North Pacific alkalinity to improve predictive algorithms. Glob. Biogeochem. Cycle 30 (10), 1493–1508.
Ganeshram, R.S., Francois, R., Commeau, J., Brown-Leger, S.L., 2003. An experimental investigation of barite formation in seawater. Geochim. Cosmochim. Acta 67 (14), 2599–2605.
GEOTRACES-Intermediate-Data-Product-Group, 2023. The GEOTRACES Intermediate Data Product 2021v2 (IDP2021v2). NERC EDS British Oceanographic Data Centre NOC.
Gonneea, M.E., Paytan, A., 2006. Phase associations of barium in marine sediments. Mar. Chem. 100 (1), 124–135.
Gonzalez-Munoz, M.T., Martinez-Ruiz, F., Morcillo, F., Martin-Ramos, J.D., Paytan, A., 2012. Precipitation of barite by marine bacteria: a possible mechanism for marine barite formation. Geology 40 (8), 675–678.
Griffith, E.M., Paytan, A., 2012. Barite in the ocean - occurrence, geochemistry and palaeoceanographic applications. Sedimentology 59 (6), 1817–1835.
Hautala, S.L., 2018. The abyssal and deep circulation of the Northeast Pacific Basin. Prog. Oceanogr. 160, 68–82.
Hodell, D.A., Mead, G.A., Mueller, P.A., 1990. Variation in the strontium isotopic composition of seawater (8 Ma to present): Impications for chemical weathering rates and dissolved fluxes to the oceans. Chem. Geol. 80 (4), 291–307.
Horner, T.J., Crockford, P.W., 2021. Barium isotopes: Drivers, dependencies, and distributions through space and time. Cambridge University Press, Cambridge.
Horner, T.J., Kinsley, C.W., Nielsen, S.G., 2015. Barium-isotopic fractionation in seawater mediated by barite cycling and oceanic circulation. Earth Planet. Sci. Lett. 430, 511–522.
Horner, T.J., Pryer, H.V., Nielsen, S.G., Crockford, P.W., Gauglitz, J.M., Wing, B.A., Ricketts, R.D., 2017. Pelagic barite precipitation at micromolar ambient sulfate. Nat. Comms. 8 (1), 1342.
Hou, Y., Hammond, D.E., Berelson, W.M., Kemnitz, N., Adkins, J.F., Lunstrum, A., 2019. Spatial patterns of benthic silica flux in the North Pacific reflect upper ocean production. Deep-Sea Res. I 148, 25–33.
Hsieh, Y.-T., Henderson, G.M., 2017. Barium stable isotopes in the global ocean: Tracer of Ba inputs and utilization. Earth Planet. Sci. Lett. 473, 269–278.
Jacquet, S.H.M., Henjes, J., Dehairs, F., Worobiec, A., Savoye, N., Cardinal, D., 2007a. Particulate Ba-barite and acantharians in the Southern Ocean during the European Iron Fertilization Experiment (EIFEX). J. Geophys. Res. Biogeo. 112, G04006.
Jacquet, S.H.M., Dehairs, F., Elskens, M., Savoye, N., Cardinal, D., 2007b. Barium cycling along WOCE SR3 line in the Southern Ocean. Mar. Chem. 106 (1), 33–45.
Kemnitz, N., Hammond, D.E., Henderson, P., Le Roy, E., Charette, M., Moore, W., Anderson, R.F., Fleisher, M.Q., Leal, A., Black, E., Hayes, C.T., Adkins, J., Berelson, W., Bian, X., 2022. Actinium and radium fluxes from the seabed in the northeast Pacific Basin. Mar. Chem. 104180.
Krumgalz, B.S., 1982. Calcium distribution in the world ocean waters. Oceanol. Acta 5 (1), 121–128.
Lam, P. J., Lee, J., Amaral, V. J., Laubach, A., Carracino, N., Rojas, S., Mateos, K., 2024. Size-fractionated major, minor, & trace particle composition and concentration from Leg 1 (Seattle, WA to Hilo, HI) of the US GEOTRACES Pacific Meridional Transect (PMT) cruise (GP15, RR1814) on R/V Roger Revelle from Sept to Oct 2018. Biological and Chemical Oceanography Data Management Office (BCO-DMO). (Version 1) Version Date 2024-01-30.
Langer, G., Nehrke, G., Thoms, S., Stoll, H., 2009. Barium partitioning in coccoliths of Emiliania huxleyi. Geochim. Cosmochim. Acta 73 (10), 2899–2906.
Le Roy, E., Sanial, V., Charette, M.A., van Beek, P., Lacan, F., Jacquet, S.H.M., Henderson, P.B., Souhaut, M., García-Ibáñez, M.I., Jeandel, C., Pérez, F.F., Sarthou, G., 2018. The ^{226}Ra–Ba relationship in the North Atlantic during GEOTRACES-GA01. Biogeosciences 15 (9), 3027–3048.
Le Roy, E., Charette, M.A., Henderson, P.B., Shiller, A.M., Moore, W.S., Kemnitz, N., Hammond, D.E., Horner, T.J., 2024. Controls on dissolved barium and radium-226 distributions in the Pacific Ocean along GEOTRACES GP15. Glob. Biogeochem. Cycle 38 (6).
Lea, D., Boyle, E., 1989. Barium content of benthic foraminifera controlled by bottom-water composition. Nature 338 (6218), 751–753.
Lebrato, M., Garbe-Schönberg, D., Müller, M.N., Blanco-Ameijeiras, S., Feely, R.A., Lorenzoni, L., Molinero, J.-C., Bremer, K., Jones, D.O.B., Iglesias-Rodriguez, D., Greeley, D., Lamare, M.D., Paulmier, A., Graco, M., Cartes, J., Barcelos e Ramos, J., de Lara, A., Sanchez-Leal, R., Jimenez, P., Paparazzo, F.E., Hartman, S.E., Westernströer, U., Küter, M., Benavides, R., da Silva, A.F., Bell, S., Payne, C., Olafsdottir, S., Robinson, K., Jantunen, L.M., Korablev, A., Webster, R.J., Jones, E. M., Gilg, O., Bailly du Bois, P., Beldowski, J., Ashjian, C., Yahia, N.D., Twining, B., Chen, X.-G., Tseng, L.-C., Hwang, J.-S., Dahms, H.-U., Oschlies, A., 2020. Global variability in seawater Mg:Ca and Sr:Ca ratios in the modern ocean. PNAS, 201918943.
Lecuyer, C., 2016. Seawater residence times of some elements of geochemical interest and the salinity of the oceans. Bull. Soc. Geol. Fr. 187 (6), 245–259.
Light, T., Martínez-Ruiz, F., Norris, R., 2023. Marine barite morphology as an indicator of biogeochemical conditions within organic matter aggregates. Geochim. Cosmochim. Acta 358, 38–48.
Light, T., Norris, R., 2021. Quantitative visual analysis of marine barite microcrystals: Insights into precipitation and dissolution dynamics. Limnol. Oceanogr. 66 (10), 3619–3629.
Martin, P., Allen, J.T., Cooper, M.J., Johns, D.G., Lampitt, R.S., Sanders, R., Teagle, D.A. H., 2010. Sedimentation of acantharian cysts in the Iceland Basin: Strontium as a ballast for deep ocean particle flux, and implications for acantharian reproductive strategies. Limnol. Oceanogr. 55 (2), 604–614.
Martinez-Ruiz, F., Paytan, A., Gonzalez-Muñoz, M.T., Jroundi, F., Abad, M.M., Lam, P.J., Bishop, J.K.B., Horner, T.J., Morton, P.L., Kastner, M., 2019. Barite formation in the ocean: origin of amorphous and crystalline precipitates. Chem. Geol. 511, 441–451.
Massera Bottazzi, E., Schreiber, B., Bowen, V.T., 1971. Acantharia in the Atlantic Ocean, Their Abundance and Preservation. Limnol. Oceanogr. 16 (4), 677–684.
McDougall, T.J., Barker, P.M., 2011. Getting started with TEOS-10 and the Gibbs Seawater (GSW) Oceanographic Toolbox. SCOR/IAPSO WG127, p. 28.
Mete, Ö.Z., Subhas, A.V., Kim, H.H., Dunlea, A.G., Whitmore, L.M., Shiller, A.M., Gilbert, M., Leavitt, W.D., Horner, T.J., 2023. Barium in seawater: dissolved distribution, relationship to silicon, and barite saturation state determined using machine learning. Earth Syst. Sci. Data 15 (9), 4023–4045.
Meyer, E.M., Langer, G., Brownlee, C., Wheeler, G.L., Taylor, A.R., 2020. Sr in coccoliths of Scyphosphaera apsteinii: Partitioning behavior and role in coccolith morphogenesis. Geochim. Cosmochim. Acta 285, 41–54.
Michaels, A.F., 1988. Vertical distribution and abundance of Acantharia and their symbionts. Mar. Biol. 97 (4), 559–569.
Michaels, A.F., 1991. Acantharian abundance and symbiont productivity at the VERTEX seasonal station. J. Plankton Res. 13 (2), 399–418.
Michaels, A.F., Caron, D.A., Swanberg, N.R., Howse, F.A., Michaels, C.M., 1995. Planktonic sarcodines (Acantharia, Radiolaria, Foraminifera) in surface waters near Bermuda: abundance, biomass and vertical flux. J. Plankton Res. 17 (1), 131–163.
Middleton, J.T., Paytan, A., Auro, M., Saito, M.A., Horner, T.J., 2023. Barium isotope signatures of barite–fluid ion exchange in Equatorial Pacific sediments. Earth Planet. Sci. Lett. 612, 118150.
Millero, F.J., Feistel, R., Wright, D.G., McDougall, T.J., 2008. The composition of Standard Seawater and the definition of the Reference-Composition Salinity Scale. Deep-Sea Res. Pt. I 55 (1), 50–72.
Milliman, J.D., 1974. Marine carbonates. Springer-Verlag, Berlin.
Monnin, C., Cividini, D., 2006. The saturation state of the world's ocean with respect to (Ba, Sr)S_O4 solid solutions. Geochim. Cosmochim. Acta 70 (13), 3290–3298.
Monnin, C., Jeandel, C., Cattaldo, T., Dehairs, F., 1999. The marine barite saturation state of the world's oceans. Mar. Chem. 65 (3–4), 253–261.
Moore, W.S., 1997. High fluxes of radium and barium from the mouth of the Ganges-Brahmaputra River during low river discharge suggest a large groundwater source. Earth Planet. Sci. Lett. 150 (1), 141–150.
Murray, J.W., 1975. The interaction of metal ions at the manganese dioxide-solution interface. Geochim. Cosmochim. Acta 39 (4), 505–519.
Paytan, A., Griffith, E.M., 2007. Marine barite: recorder of variations in ocean export productivity. Deep-Sea Res. Pt. II 54 (5–7), 687–705.
Paytan, A., Griffith, E.M., Eisenhauer, A., Hain, M., Wallmann, K., Ridgwell, A., 2021. A 35 Myr Record of Seawater Stable Sr Isotopes Reveals a Fluctuating Global Carbon Cycle. Science 371 (6536), 1346–1350.
Paytan, A., Kastner, M., 1996. Benthic Ba fluxes in the central Equatorial Pacific, implications for the oceanic Ba cycle. Earth Planet. Sci. Lett. 142 (3–4), 439–450.
Paytan, A., Kastner, M., Chavez, F.P., 1996. Glacial to interglacial fluctuations in productivity in the equatorial Pacific as indicated by marine barite. Science 274 (5291), 1355–1357.
Pilátová, J., Tashyreva, D., Týč, J., Vancová, M., Bokhari, S.N.H., Skoupý, R., Klementová, M., Küpper, H., Mojzeš, P., Lukeš, J., 2023. Massive accumulation of strontium and barium in diplonemid protists. mBio.
Rahman, S., Shiller, A.M., Anderson, R.F., Charette, M.A., Hayes, C.T., Gilbert, M., Grissom, K.R., Lam, P.J., Ohnemus, D.C., Pavia, F.J., Twining, B.S., Vivancos, S.M., 2022. Dissolved and particulate barium distributions along the US GEOTRACES North Atlantic and East Pacific zonal transects (GA03 and GP16): Global implications for the marine barium cycle. Glob. Biogeochem. Cycle 36 (6).
Richter, F.M., Turekian, K.K., 1993. Simple models for the geochemical response of the ocean to climatic and tectonic forcing. Earth Planet. Sci. Lett. 119 (1–2), 121–131.
Rushdi, A.I., McManus, J., Collier, R.W., 2000. Marine barite and celestite saturation in seawater. Mar. Chem. 69 (1–2), 19–31.
Sarmiento, J.L., Simeon, J., Gnanadesikan, A., Gruber, N., Key, R.M., Schlitzer, R., 2007. Deep ocean biogeochemistry of silicic acid and nitrate. Glob. Biogeochem. Cycle 21 (1).
Schiebel, R., Hemleben, C., 2017. Planktic Foraminifers in the Modern Ocean, second ed. Springer-Verlag, Berlin Heidelberg.
Schlitzer, R., 2020. Ocean Data View. https://odv.awi.de.
Schrag, D.P., 1999. Rapid analysis of high-precision Sr/Ca ratios in corals and other marine carbonates. Paleoceanography 14 (2), 97–102.
Steiner, Z., Turchyn, A.V., Harpaz, E., Silverman, J., 2018. Water chemistry reveals a significant decline in coral calcification rates in the southern Red Sea. Nat. Comms. 9 (1), 3615.
Steiner, Z., Sarkar, A., Prakash, S., Vinayachandran, P.N., Turchyn, A.V., 2020. Dissolved strontium, Sr/Ca ratios, and the abundance of Acantharia in the Indian and Southern Oceans. ACS Earth Space Chem. 4 (6), 802–811.
Steiner, Z., Sarkar, A., Liu, X., Berelson, W.M., Adkins, J.F., Prabhakaran, S., Prakash, S., Vinaychandran, P.N., Byrne, R.H., Turchyn, A.V., 2021. On calcium-to-alkalinity

anomalies in the North Pacific, Red Sea, Indian Ocean and Southern Ocean. Geochim. Cosmochim. Acta 303, 1–14.
Steiner, Z., Landing, W.M., Bohlin, M.S., Greaves, M., Prakash, S., Vinayachandran, P.N., Achterberg, E.P., 2022a. Variability in the concentration of lithium in the Indo-Pacific Ocean. Glob. Biogeochem. Cycle 36 (6).
Steiner, Z., Rae, J.W.B., Berelson, W.M., Adkins, J.F., Hou, Y., Dong, S., Lampronti, G.I., Liu, X., Achterberg, E.P., Subhas, A.V., Turchyn, A.V., 2022b. Authigenic formation of clay minerals in the abyssal North Pacific. Glob. Biogeochem. Cycle 36 (11).
Steiner, Z., Antler, G., Berelson, W.M., Crockford, P.W., Dunlea, A.G., Hou, Y., Adkins, J. F., Turchyn, A.V., Achterberg, E.P., 2023. Trace element geochemistry in North Pacific red clay sediment porewaters and implications for water-column studies. Glob. Biogeochem. Cycle 37 (11).
Sternberg, E., Tang, D.G., Ho, T.Y., Jeandel, C., Morel, F.M.M., 2005. Barium uptake and adsorption in diatoms. Geochim. Cosmochim. Acta 69 (11), 2745–2752.
Stoll, H.M., Schrag, D.P., 2000. Coccolith Sr/Ca as a new indicator of coccolithophorid calcification and growth rate. Geochem. Geophys. Geosyst. 1 (5).
Stoll, H.M., Ziveri, P., 2004. Coccolithophorid-based geochemical paleoproxies. In: Thierstein, H.R., Young, J.R. (Eds.), Coccolithophores: from Molecular Processes to Global Impact. Springer, Berlin Heidelberg, Berlin, Heidelberg, pp. 529–562.
Stoll, H.M., Ziveri, P., Shimizu, N., Conte, M., Theroux, S., 2007. Relationship between coccolith Sr/Ca ratios and coccolithophore production and export in the Arabian Sea and Sargasso Sea. Deep-Sea Res. II 54 (5–7), 581–600.
Toggweiler, J.R., Druffel, E.R.M., Key, R.M., Galbraith, E.D., 2019. Upwelling in the Ocean Basins North of the ACC: 1. On the Upwelling Exposed by the Surface Distribution of Δ14C. J. Geophys. Res. Oceans 124 (4), 2591–2608.
Torres-Crespo, N., Martínez-Ruiz, F., González-Muñoz, M.T., Bedmar, E.J., De Lange, G. J., Jroundi, F., 2015. Role of bacteria in marine barite precipitation: a case study using Mediterranean seawater. Sci. Total Environ. 512–513, 562–571.
van Beek, P., François, R., Honda, M., Charette, M.A., Reyss, J.-L., Ganeshram, R., Monnin, C., Honjo, S., 2022. Fractionation of ^{226}Ra and Ba in the Upper North Pacific Ocean. Front. Mar. Sci. 9.
van Beek, P., Reyss, J.L., Bonte, P., Schmidt, S., 2003. Sr/Ba in barite: a proxy of barite preservation in marine sediments? Mar. Geol. 199 (3), 205–220.
van Beek, P., François, R., Conte, M., Reyss, J.L., Souhaut, M., Charette, M., 2007. ^{228}Ra/^{226}Ra and ^{226}Ra/Ba ratios to track barite formation and transport in the water column. Geochim. Cosmochim. Acta 71 (1), 71–86.
Whitmore, L.M., Shiller, A.M., Horner, T.J., Xiang, Y., Auro, M.E., Bauch, D., Dehairs, F., Lam, P.J., Li, J., Maldonado, M.T., Mears, C., Newton, R., Pasqualini, A., Planquette, H., Rember, R., Thomas, H., 2022. Strong margin Influence on the Arctic Ocean barium cycle revealed by pan-Arctic synthesis. J. Geophys. Res. Oceans 127 (4).
Wu, J., Liu, Z., Michard, A., Tachikawa, K., Filippidi, A., He, Z., Hennekam, R., Yang, S., Davies, G.R., de Lange, G.J., 2022. Effect of barite-bound Sr on detrital Sr isotope systematics in marine sediments. Chem. Geol. 587, 120613.
Yu, Y., Xie, R.C., Gutjahr, M., Laukert, G., Cao, Z., Hathorne, E., Siebert, C., Patton, G., Frank, M., 2022. High latitude controls on dissolved barium isotope distributions in the global ocean. Geochem. Perspect. Lett. 24, 22–26.
Zheng, L., Minami, T., Konagaya, W., Chan, C.-Y., Tsujisaka, M., Takano, S., Norisuye, K., Sohrin, Y., 2019. Distinct basin-scale-distributions of aluminum, manganese, cobalt, and lead in the North Pacific Ocean. Geochim. Cosmochim. Acta 254, 102–121.
Zheng, L., Minami, T., Takano, S., Ho, T.-Y., Sohrin, Y., 2021. Sectional distribution patterns of Cd, Ni, Zn, and Cu in the North Pacific Ocean: Relationships to nutrients and importance of scavenging. Glob. Biogeochem. Cycle 35 (7).
Ziveri, P., Gray, W.R., Anglada-Ortiz, G., Manno, C., Grelaud, M., Incarbona, A., Rae, J. W.B., Subhas, A.V., Pallacks, S., White, A., Adkins, J.F., Berelson, W., 2023. Pelagic calcium carbonate production and shallow dissolution in the North Pacific Ocean. Nat. Comms. 14 (1), 805.